Chemico-Biological Interactions 238 (2015) 102–110

Contents lists available at ScienceDirect

Chemico-Biological Interactions

journal homepage: www.elsevier.com/locate/chembioint

A preliminary regional PBPK model of lung metabolism for improving species dependent descriptions of 1,3-butadiene and its metabolites

Jerry Campbell [a], Cynthia Van Landingham [b,*], Susan Crowell [c], Robinan Gentry [b], Debra Kaden [d], Stacy Fiebelkorn [e], Anne Loccisano [f], Harvey Clewell [a,b]

[a] The Hamner Institutes for Health Research, Research Triangle Park, NC, USA
[b] Ramboll Environ, 1900 N. 18th St., Suite 804, Monroe, LA 71201, USA
[c] Pacific Northwest National Laboratory, 902 Battelle Boulevard, Richland, WA 99352, USA
[d] Ramboll Environ, 20 Custom House Street, Suite 800, Boston, MA 02110, USA
[e] British American Tobacco (Investments) Ltd, Research and Development, Regents Park Road, Southampton SO15 8TL, UK
[f] R.J. Reynolds Tobacco Company, P.O. Box 1487, Winston-Salem, NC 27102, USA

ARTICLE INFO

Article history:
Received 8 December 2014
Received in revised form 14 May 2015
Accepted 26 May 2015
Available online 12 June 2015

Keywords:
1,3-Butadiene
Physiologically – based pharmacokinetic model
PBPK
Lung metabolism

ABSTRACT

1,3-Butadiene (BD), a volatile organic chemical (VOC), is used in synthetic rubber production and other industrial processes. It is detectable at low levels in ambient air as well as in tobacco smoke and gasoline vapors. Inhalation exposures to high concentrations of BD have been associated with lung cancer in both humans and experimental animals, although differences in species sensitivity have been observed. Metabolically active lung cells such as Pulmonary Type I and Type II epithelial cells and club cells (Clara cells)[1] are potential targets of BD metabolite-induced toxicity. Metabolic capacities of these cells, their regional densities, and distributions vary throughout the respiratory tract as well as between species and cell types. Here we present a physiologically based pharmacokinetic (PBPK) model for BD that includes a regional model of lung metabolism, based on a previous model for styrene, to provide species-dependent descriptions of BD metabolism in the mouse, rat, and human. Since there are no *in vivo* data on BD pharmacokinetics in the human, the rat and mouse models were parameterized to the extent possible on the basis of *in vitro* metabolic data. Where it was necessary to use *in vivo* data, extrapolation from rat to mouse was performed to evaluate the level of uncertainty in the human model. A kidney compartment and description of downstream metabolism were also included in the model to allow for eventual use of available urinary and blood biomarker data in animals and humans to calibrate the model for estimation of BD exposures and internal metabolite levels. Results from simulated inhalation exposures to BD indicate that incorporation of differential lung region metabolism is important in describing species differences in pulmonary response and that these differences may have implications for risk assessments of human exposures to BD.

1. Introduction

1,3-Butadiene (BD)[2] (CAS No. 106-99-0) is a colorless and mildly aromatic gas. It is commonly used in the manufacturing of tires, shoes, sponges, hoses, luggage, and a variety of molded products [61]. BD is also a constituent of tobacco smoke, gasoline vapors, and vapors from the burning of plastics and rubber, and has been detected at low part-per-billion levels in outdoor air [43]. BD is a

* Corresponding author. Tel.: +1 318 398 2091.
E-mail addresses: jcampbell@thehamner.org (J. Campbell), cvanlandingham@environcorp.com (C. Van Landingham), susan.r.crowell@gmail.com (S. Crowell), rgentry@environcorp.com (R. Gentry), dkaden@environcorp.com (D. Kaden), Stacy_Fiebelkorn@bat.com (S. Fiebelkorn), loccisa@rjrt.com (A. Loccisano), hclewell@environcorp.com (H. Clewell).

[1] Based on the suggestions in Winkelmann and Noack (2010) [63] and Irwin et al. (2013) [25], bronchiolar exocrine cells (Clara cells) will be referred to as club cells in this paper.

[2] *Abreviations used:* BD, 1,3-butadiene; VOC, volatile organic chemical; PBPK, physiologically based pharmacokinetic; EB, epoxybutene; DEB, 1,2,3,4-diepoxybutane; CYP, cytochrome P450; GST, glutathione-S-transferase; M2, an isomeric mixture of 1-hydroxy-2-(N-acetylcysteinyl)-3-butene and 2-hydroxy-1-(N-acetylcysteinyl)-3-butene; EH, epoxide hydrolase; BD-diol, 1,2-dihydroxy-3-butene or epoxybutanediol; HMVK, hydroxymethylvinyl ketone; M1, 1,2-dihydroxy-4-(N-acetylcysteinyl)-butane; V_{max}, maximal velocity; K_m, substrate concentration at which the reaction rate is half of V_{max}; GSH, glutathione; RAgshT, rate equation for GSH levels; kPgshT, tissue specific zero order rate of GSH synthesis; kEgsh, first order rate of basal GSH elimination; VT, tissue volume; CgshT, tissue concentration of GSH; RAMTgsh, rate of conjugation of GSH and EB; PNNL, Pacific Northwest National Laboratory.

http://dx.doi.org/10.1016/j.cbi.2015.05.025
0009-2797/

known human carcinogen [23] and has been associated with cancer in multiple sites [19], as well as non-carcinogenic outcomes, notably reproductive toxicity in animals [11]. Studies have shown that mice are much more sensitive to BD toxicity than rats, due at least in part to species-specific kinetic differences between rats and mice, and differences between mice and humans [19]. The carcinogenicity and toxicity observed from BD exposure have been attributed to its epoxide metabolites, 1,2-epoxy-3-butene (epoxybutene, EB) and 1,2,3,4-diepoxybutane (DEB).

BD is activated primarily by cytochrome P450 2E1 (CYP 2E1) to produce the genotoxic metabolites EB and DEB [1,6,29]. These reactive epoxide metabolites can form hemoglobin adducts and are believed to be responsible for BD-induced genotoxicity and carcinogenicity, as well as the non-carcinogenic effects. EB is then further metabolized by three different pathways: conjugation by glutathione-S-transferase (GST) to form the urinary metabolite M2 (an isomeric mixture of 1-hydroxy-2-(N-acetylcysteinyl)-3-butene and 2-hydroxy-1-(N-acetylcysteinyl)-3-butene), hydrolyzation by epoxide hydrolase (EH) to 1,2-dihydroxy-3-butene (epoxybutanediol, BD-diol), and finally oxidation to the more genotoxic metabolite, DEB, by cytochrome P450 (Fig. 1).

BD-diol is further metabolized in multiple steps by alcohol dehydrogenase, aldehyde dehydrogenase, and cytochrome P450 to form the intermediate hydroxymethylvinyl ketone (HMVK), which is then further conjugated by GST to form the urinary metabolite, M1 (1,2-dihydroxy-4-(N-acetylcysteinyl)-butane).

In addition to the liver, the lung and kidney have been shown to be sites of BD metabolism, as well as target sites for tissue damage and carcinogenicity in rodents [12,26,56]. In pulmonary tissues, epithelial cells (Pulmonary Type I and Type II) and club cells (based on the suggestions in Winkelmann and Noack (2010) [63] and Irwin et al. (2013) [25], bronchiolar exocrine cells or Clara cells will be referred to as club cells) are the primary metabolically active cells and potential targets of BD epoxide metabolite-induced toxicity and carcinogenicity [19]. However, metabolic capacities, regional densities, and the distribution of these cells vary throughout the respiratory tract and across different species [55].

In mice, metabolically active cells can be found at all levels of the respiratory tract [49,46,45,51], while in rats and humans they are confined to the transitional airways immediately before the alveolar regions of the lung [47,51,42]. This, along with the increased rates of metabolic activation of BD in the respiratory tissues of mice [12,16,56,7,15,38,36,35], may be the reason for the greater susceptibility of mice, compared to rats, to BD-induced pulmonary toxicity and carcinogenicity [19]. Therefore, it is important to include a more complex description of the respiratory tract in a PBPK model to adequately account for the species-specific differences and the complex activation of BD in the lung.

Numerous PBPK models for BD and its metabolites have been developed and are available in the published literature (Table A-1) [28,40,13,34,59]. However, the existing BD inhalation PBPK models treat the lung as a homogenous organ with metabolism occurring evenly throughout, despite known differences in lung physiology and metabolic capacity across respiratory regions and between species. Therefore, these models insufficiently elucidate species-specific differences in the lung metabolism of BD to support cross-species extrapolation of lung cancer risk.

The aim of the BD PBPK model presented here for mice, rats, and humans is to more accurately model inhalation exposure to BD using an expanded description of the lung compartment first used for styrene [55]. The model described here distributes the metabolism to specific sub-divided regions with distinct metabolic characteristics – oral/nasal passage, conducting airways (trachea, bronchi, and anterior bronchioles), transitional airways (terminal bronchioles), and the alveolar gas exchange region – and provides the capability to estimate region-specific dosimetry. The model also includes a more detailed and complex description of metabolism of BD by the inclusion of a kidney compartment and metabolite sub-models, which will allow for consideration of available

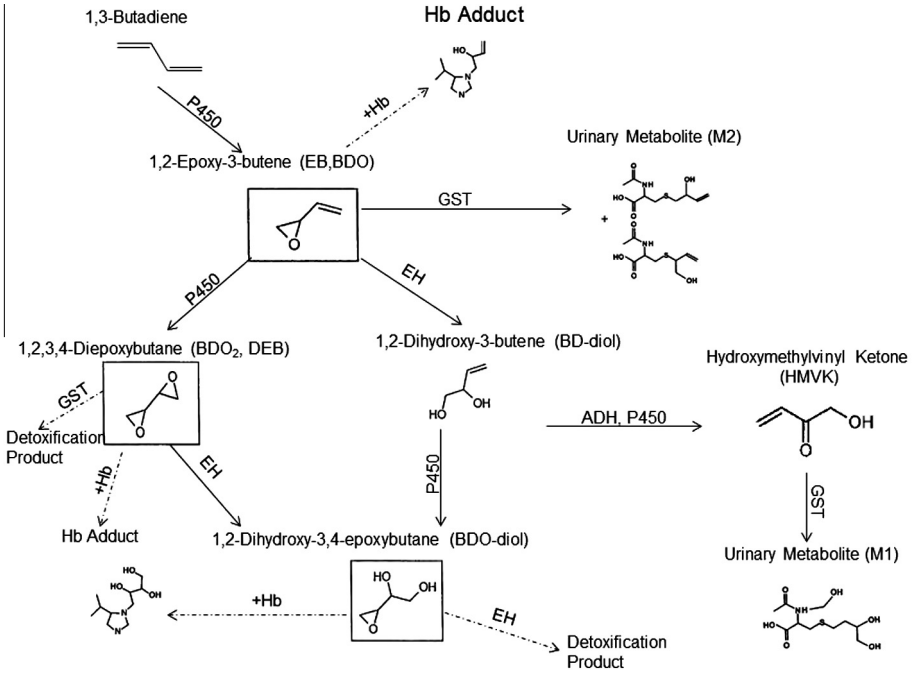

Fig. 1. A simplified metabolic scheme for BD showing the metabolism modeled. A box around the chemical structure indicates it is a reactive epoxide metabolite, and broken lines indicate planned additions to the model. EH – epoxide hydrolase, GST – glutathione-S-transferase, P450 – cytochrome P450. Note: there are multiple urinary metabolites that are not referenced in this simplified scheme.

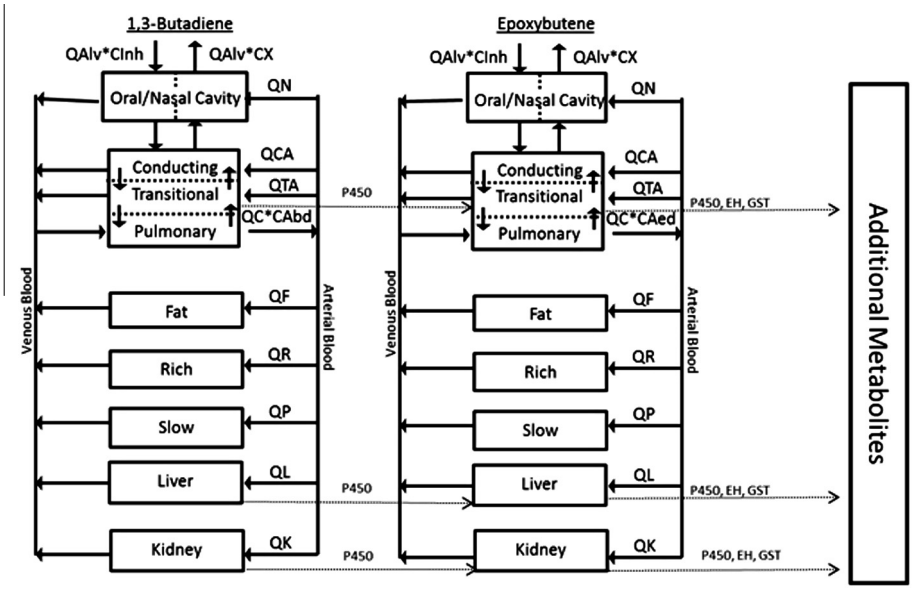

Fig. 2. Basic structure of PBPK model for BD and its major metabolite, epoxybutene (EB). Additional metabolites are also modeled but not shown explicitly. In the mouse, metabolically active cells are distributed in both the conducting and transitional airways, but in humans and rats, they are present only in the transitional airways.

urinary biomarker data in animals and humans in model calibration and will more accurately describe the metabolism of BD.

2. Methods

2.1. PBPK model structure

The inhalation PBPK model for BD was written in acslX (version 3.0, Aegis Corporation, Huntsville, AL, USA). The Gear algorithm was used for integration of double precision variables. The PBPK model contains seven compartments representing the liver, kidney, fat, richly perfused tissues, slowly perfused tissues, oral/nasal cavity, and multi-compartment lung, connected via arterial and venous blood (Fig. 2).

Sub-models of EB and BD-diol were also included to track the metabolism of BD. The lung compartment was divided into four main regions – the nasal cavity, conducting airways, transitional airways, and the alveolar gas exchange region. With the exception of the nasal cavity, each level of the respiratory tract is separated into the lumen, epithelial cells, and submucosa tissues (Fig. 3). The nasal cavity airways are comprised of the lumen and nasal tissue. Cytochrome P450 metabolism in the lung is limited to certain epithelial cells: Type I, Type II, and club cells [51]. A complete description of the respiratory architecture employed in this PBPK model can be found in Sarangapani and Teeguarden [55].

The metabolic description was based on that described in previous BD model efforts [33,34,28,58]. Metabolism in the pulmonary region was isolated to the transitional airway as this is the primary site of metabolically active cells in human respiratory tract [47,51,42]. The model also includes a metabolically active kidney compartment to account for the metabolism of EB and BD-diol to the urinary metabolites M1 and M2, respectively [34,59]. The oxidation of BD and EB by cytochrome P450 (CYP) in the liver, kidney, and transitional airway is described as a saturable process (V_{max} and K_m) and includes competitive inhibition, as described in Kohn and Melnick [33]. The hydrolysis of EB by epoxide hydrolase (EH) is also described as a saturable process in the liver, kidney, and metabolically active areas of the lung. The "privileged access" description of Kohn and Melnick [33] was used in the liver, where colocation of the EH enzyme with the CYP enzyme results in access to metabolism prior to EB being available for partitioning to plasma. The release of bound EB (KRELEB) was adjusted to minimize the ratio of AUC calculated within the time of measured data (i.e., 120 min to final sample for plasma and 180 min to final sample time for lung) between observed and simulated EB in plasma and lung for rat. A similar rate constant of 1.4 min^{-1} provided acceptable fits to the mouse and was retained for the human. Conjugation of EB is modeled in the liver, relevant airways, and the kidney, and occurs by a ping–pong mechanism [28,13]. The rate equation for GSH level (RAgshT) is described as:

$$\mathrm{RAgshT} = \mathrm{kPgshT} - \mathrm{kEgsh} * \mathrm{VT} * \mathrm{CgshT} - \mathrm{RAMTgsh}$$

where kPgshT is the tissue-specific zero-order rate of GSH synthesis (determined from basal tissue GSH concentrations and the basal elimination rate), kEgsh is the first-order rate of basal GSH elimination, VT is the tissue volume, CgshT is the tissue concentration of GSH, and RAMTgsh is the rate of conjugation of GSH and EB. This same method was also used to describe the conjugation of the BD-diol intermediate HMVK to the urinary biomarker, M1. BD-diol is also modeled through saturable oxidation in the liver, kidney, and in only the conducting airway and transitional airway of the lung, by cytochrome P450 to form the intermediate HMVK, which is further conjugated to produce M1 in the urine (as discussed earlier).

Physiological, biochemical, and metabolic parameters used in the model are listed in Tables A-2 to A-4 for rats, mice, and humans, respectively. Metabolic parameters for the mouse and rat (Table A-4) were taken from Kohn and Melnick [33], Sweeney et al. [59], and Johanson and Filser [28] and are based on metabolic rates from *in vitro* studies of BD and EB metabolism in mouse and rat microsomes. The rate constants for humans (Table A-4) were derived from *in vitro* measurements reported in Csanády et al. [12] and employed by Sweeney et al. [59] or set to the rat value for pathways that were not assessed in human microsomal preparations. In keeping with the Kohn and Melnick [33,34] description, maximum rates of metabolism for the saturable processes were scaled to the tissue using the tissue-specific concentration of microsomal or cytosolic protein per gram of tissue [66].

2.2. Data used for model parameters

A search of the published literature, using the PubMed bibliographic database, was performed to identify studies containing

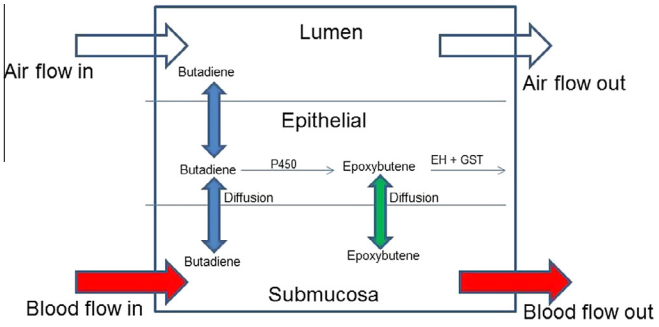

Fig. 3. Detail of the structure used to model the transitional airways.

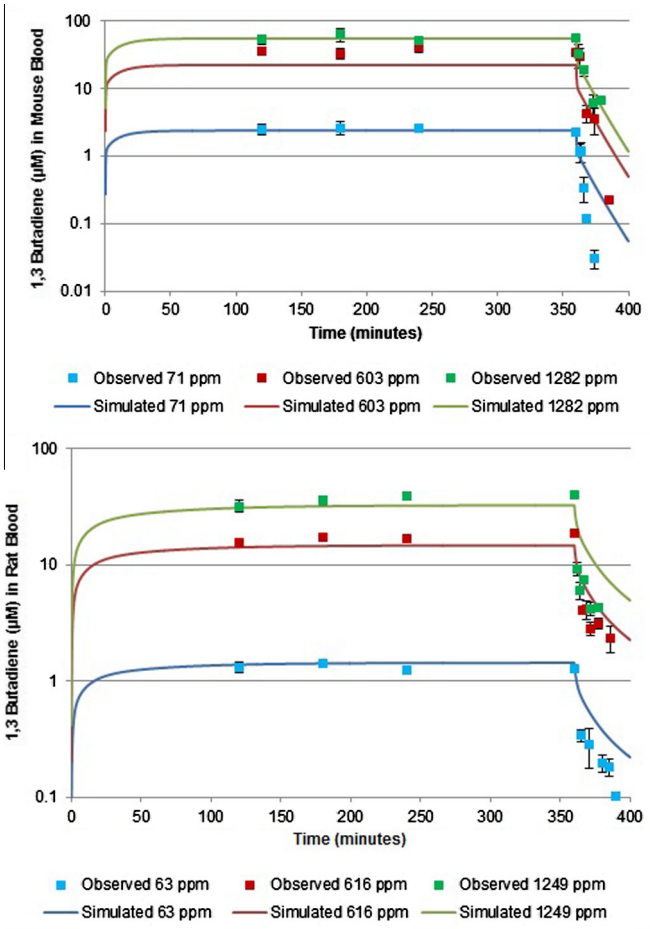

Fig. 4. BD concentrations in the blood of B63CF1 mice (top) or Sprague-Dawley rats (bottom) during and following six hours of inhalation exposure to a target concentration of 62.5 ppm, 625 ppm or 1250 ppm of BD (71 ppm, 603 ppm, or 1282 ppm in mice and 63 ppm, 616 ppm, or 1249 ppm in rats; observed data from [18]).

data for the time course concentrations of inhaled BD in the mouse, rat, or human urine and metabolic rate data for BD metabolites in the kidney, lung, and liver. Tables A-1 to A-4 summarize the relevant information identified from the literature search results that were used in the parameterization of the model for the mouse, rat, and human. Tissue volumes were scaled linearly with body weight, cardiac output was scaled as body weight to the 0.75 power, and tissue perfusion rates were set as a fraction of cardiac output. Partition coefficients and hepatic metabolic rate constants were taken from the literature. Parameters describing the structure of sub-compartments of the lung (lumen, volumes, surface area,

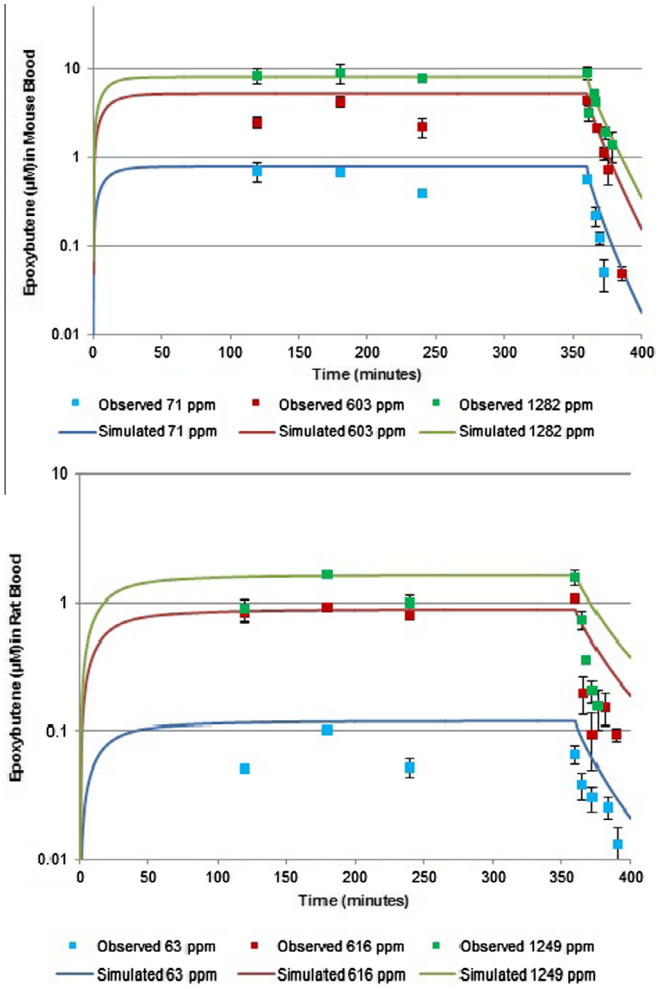

Fig. 5. EB in the blood of B63CF1 mice (top) or Sprague-Dawley rats (bottom) during and following six hours of inhalation exposure to a target concentration of 62.5 ppm, 625 ppm or 1250 ppm of BD (71 ppm, 603 ppm, or 1282 ppm in mice and 63 ppm, 616 ppm, or 1249 ppm in rats; observed data from [18]).

and tissue thickness) represent measured and estimated values from the literature and were not scaled allometrically. EPISUITE calculator version 4.10 was used to estimate the mass transfer coefficients and diffusivity constants [62].

3. Results

Model performance evaluation was conducted through comparison to published pharmacokinetic data sets, representing closed chamber and exhaled breath data, as well as measurements of BD in the blood and exhaled breath and EB in the blood and lung. The model simulations were in good agreement with clearance of various concentrations of BD or EB from closed chambers holding five or eight mice [26,37,34] and from chambers holding one or two rats [4,34] (data not shown).

The model simulation of BD in B63CF1 mouse or Sprague-Dawley rat blood during and following six hours of exposure to inhaled BD [18] was in good agreement with both the mouse data and the rat data (Fig. 4). While there is a general trend of under-predicting the post-exposure samples, the model simulation stays within a factor of 2 of nearly all the measured concentrations. Similar results are seen with EB, where the model provides good agreement with the during-exposure measure of EB in plasma but under-predicts the post-exposure clearance of EB in both mouse and rat (Fig. 5). The model stays within a factor of 3 for all but the last time-point at

Table 1
Ratio of observed to simulated $AUC_{(120\ min\text{-}t)}$ for 1,3-butadiene and expoxybutene in mice and rats exposed nose-only to butadiene for 6 h (observed: [18]).

		Ratio $AUC_{(120\ min\text{-}t)}$ (Observed:simulated)	
	Exposure (ppm)	Butadiene	Epoxybutene
Mouse	62.5	1.04	0.68
	625	1.62	0.64
	1250	1.00	1.03
Rat	62.5	0.90	1.77
	625	1.16	1.02
	1250	1.15	1.28

62.5 ppm and 625 ppm in the mouse and the terminal phase for the rat at 625 ppm and 1250 ppm. Based upon the ratio of observed $AUC_{(120\ min\text{-}t)}$ to that predicted by the model (Table 1), the ratio stays well within a factor of 2 of the observed data for both BD and EB in blood with the highest ratio being 1.62 at 62.5 ppm in the mouse. The human exhaled concentrations of BD [3] were well-predicted by the model (Fig. 6).

4. Conclusions

A preliminary PBPK model for BD in mice, rats, and humans has been developed, which includes regional generation of reactive metabolites in the lung and metabolism in the kidney, as well as the hepatic metabolism used in most existing PBPK models of BD. Previous PBPK models have focused on hepatic metabolism and systemically circulating reactive metabolites. Here, a PBPK model has been developed to incorporate species differences in the distribution of metabolically active club cells throughout the pulmonary tissues. The complex pulmonary metabolism and addition of metabolism in the kidney in the model have little impact on systemic concentrations of BD or EB, but are likely to have a significant impact on local concentrations of reactive metabolites, as was observed in the case of styrene [55].

Despite the simplicity of BD's molecular structure, its metabolism is surprisingly complex, as can be seen from the descriptions that have been employed in the various PBPK models (Table A-1): privileged access enzyme channeling between CYP and epoxide hydrolase, ping–pong, or bi–bi kinetics for glutathione conjugation. This complexity, plus the reactivity of many of the metabolites, creates a particular challenge for conducting *in vitro* metabolism studies. Similar difficulties have been reported for chloroprene [20].

Previous PBPK models of BD have made use of a combination of *in vitro* and *in vivo* data in order to compare the pharmacokinetics and metabolism of BD between rats and mice. The goal of the present model, however, is to provide a description of BD pharmacokinetics and metabolism in the human. The challenge in developing a human PBPK model for BD is the lack of *in vivo* data in the human. Therefore, we have attempted to avoid reliance on *in vivo* data in developing our models for the mouse and rat. In particular, the metabolic parameters for the mouse and rat were based to the extent possible on *in vitro* metabolism data using *in vitro* to *in vivo* extrapolation (IVIVE, [66]), so that the human model could be similarly developed on the basis of human *in vitro* metabolism data. Where it was necessary to use *in vivo* data to estimate model parameters in the rat (e.g., to account for privileged access), we tested our assumptions regarding cross-species parameter equivalence in our extrapolation from the rat to the mouse and then

Table A-1
Primary existing models.

Original publication	Subsequent published updates	Notable model features
[27]	[28,13]	– BD and EB sub-models, with simple distributed DEB sub-model. – Saturable metabolism in liver compartment only. – Intrahepatic first-pass metabolism of EB (to describe the lower-than-expected EB concentrations in blood). – Epoxide–GSH conjugation described with ping–pong kinetics.
[31]	[32–34,30]	– BD, EB, DEB sub-models. – Blood compartment divided into arterial, venous, and tissue capillary beds. – Saturable metabolism in liver, lung, and kidney. – Privileged access enzyme channeling between P450 and epoxide hydrolase resulting in enhanced hydrolysis of epoxide metabolites. – Epoxide–GSH conjugation described with bi–bi kinetics.
[40]	[5,57–59,26]	– BD, EB, DEB sub-models. – Saturable metabolism in liver and lung. – Non-enzymatic elimination of EB and DEB. – BD metabolism occurs by multiple enzymes (i.e., EB-producing and other(s)).
[3]	[8,2]	– Human lifetime model with 22–41 compartments (non-pregnant vs. pregnant). – First order metabolism in liver, lung, gut, placenta. – Pulmonary, fecal, urinary, and lactational excretion.

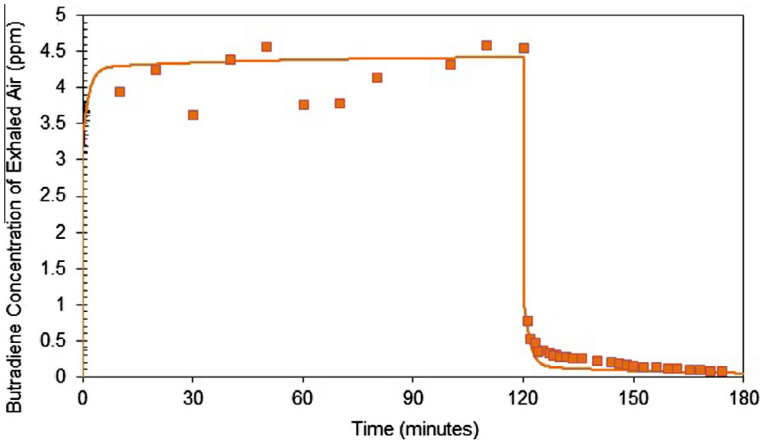

Fig. 6. Simulation of the 1,3-butadiene concentration in exhaled breath of a human subject exposed to 5 ppm for 120 min (observed data from [3]).

Table A-2
Physiological parameters.

Parameter	Symbol	Units	Rat	Mouse	Human	Refs.
Minute ventilation rate	MVC	ml/min	1.909	2.415	3.228	[9]
Cardiac output	QCC	ml/min	1.756	1.253	1.547	[9]
Fractional blood flow to fat	QFC	(% QCC)	0.07	0.059	0.052	[9]
Fractional blood flow to liver	QLC	(% QCC)	0.183	0.161	0.227	[9]
Fractional blood flow to kidney	QKC	(% QCC)	0.133	0.091	0.175	[34,9]
Fractional blood flow to richly perfused tissues	QRC	(% QCC)	0.40	0.48	0.43	[9]
Fractional blood flow to nasal tissues	QNC	(% QCC)	0.001	0.01	0.00247	[21]
Fractional blood flow to conducting airways	QCAC	(% QCC)	0.021	0.005	0.025	[9]
Fractional blood flow to transitional airways	QTAC	(% QCC)	0.0015	0.001	0.007	[10]
Body weight	BW	g	250	25	70,000	[9]
Blood volume	VBC	(% BW)	0.075	0.049	0.079	[9]
Fat volume	VFC	(% BW)	0.065	0.070	0.2143	[9]
Liver volume	VLC	(% BW)	0.037	0.055	0.0257	[9]
Kidney volume	VKC	(% BW)	0.015	0.0167	0.0044	[34,9]
Slowly perfused tissue volume	VPC	(% BW)	0.60	0.60	0.5	[9]
Nasal lumen volume	VNL	Ml	0.25	0.03	9.96	[21]
Conducting airway lumen volume	VCAL	Ml	1.13	0.11	95.7	[41]
Transitional airway lumen volume	VTAL	Ml	0.028	0.00087	61	[41]
Fraction of cell volume filled by ER	FACTOR	–	0.10	0.10	0.10	Estimated
Surface area of nasal tissues	SAN	cm^2	13.25	2.70	137.7	[21]
Surfaces area of conducting airways	SACA	cm^2	48.30	8.87	2770	[24,44,64]
Surface area of transitional airways	SATA	cm^2	5.50	0.48	6220	[24,44,64]
Surface area of pulmonary region	SAPUL	cm^2	3400	500	540,000	[60]
Mucus thickness	WMUC	cm	0.001	0.001	0.001	[52]
Nasal tissue thickness	WTN	cm	0.005	0.005	0.0049	[21]
Conducting airways epithelium thickness	WTCA	cm	0.0013	0.0013	0.003	[39]
Transitional airway epithelium thickness	WTTA	cm	0.001	0.001	0.001	[49]
Pulmonary airway epithelium thickness	WTPUL	cm	0.000038	0.000032	0.000036	[48]
Conducting airway submucosa thickness	WXCA	cm	0.005	0.005	0.0045	Estimate
Transitional airway submucosa thickness	WXTA	cm	0.002	0.002	0.002	Estimate
Tissue phase diffusivity constant	DIFFTISS	cm^2/min	0.0002	0.0002	0.0002	[14]
Air phase diffusivity constant	DIFFAIR	cm^2/min	6.42	6.42	6.42	[62]

Table A-3
Biochemical parameters.

Parameter	Symbol	Units	Rat	Mouse	Human
Blood:air partition coefficient for BD	PBBD	–	1.95[b]	1.34[a]	1.22[f]
Fat:blood partition coefficient for BD	PFBD	–	10.8[b]	14.3[a]	18.4[g]
Liver:blood partition coefficient for BD	PLBD	–	0.595[b]	1.01[a]	0.56[g]
Kidney:blood partition coefficient for BD	PKBD	–	0.472[b]	0.472[b]	0.86[g]
Poorly perfused tissue:blood partition coefficient for BD	PPBD	–	0.564[b]	2.99[a]	0.72[g]
Richly perfused tissue:blood partition coefficient for BD	PRBD	–	0.446[b]	1.01[a]	0.56[g]
Lung:blood partition coefficient for BD	PLUBD	–	0.615[b]	1.10[a]	0.39[g]
Blood:air partition coefficient for EB	PBEB	–	56.8[b]	36.6[a]	93.3[e]
Fat:blood partition coefficient for EB	PFEB	–	2.25[b]	2.49[a]	1.8[e]
Liver:blood partition coefficient for EB	PLEB	–	0.984[b]	1.15[a]	0.59[e]
Kidney:blood partition coefficient for EB	PKEB	–	0.842[b]	0.842[b]	0.59[e]
Slowly perfused tissue:blood partition coefficient for EB	PPEB	–	0.736[b]	0.64[a]	0.49[e]
Richly perfused tissue:blood partition coefficient for EB	PREB	–	0.908[b]	1.53[a]	0.59[e]
Lung:blood partition coefficient for EB	PLUEB	–	0.977[b]	1.53[a]	0.59[e]
Fat:blood partition coefficient for BD-diol	PFBDIOL	–	0.573[b]	0.573[b]	0.573[b]
Liver:blood partition coefficient for BD-diol	PLBDIOL	–	1.04[b]	1.04[b]	1.04[b]
Kidney:blood partition coefficient for BD-diol	PKBDIOL	–	0.962[b]	0.962[b]	0.962[b]
Slowly perfused tissue:blood partition coefficient for BD-diol	PPBDIOL	–	1.139[b]	1.139[b]	1.139[b]
Richly perfused tissue:blood partition coefficient for BD-diol	PRBDIOL	–	1.22[b]	1.22[b]	1.22[b]
Lung:blood partition coefficient for BD-diol	PLUBDIOL	–	1.107[b]	1.107[b]	1.107[b]
Gas phase mass transfer coefficient for nasal airways	KGN	cm/min	20887.0[c]	21088.0[c]	277.0[c]
Gas phase mass transfer coefficient for conducting airway	KGCA	cm/min	228.0[d]	312.0[d]	181.0[d]
Gas phase mass transfer coefficient for transitional airway	KGTA	cm/min	481.0[d]	1136.0[d]	158.0[d]

[a] [58].
[b] [34].
[c] [21].
[d] [14].
[e] [13].
[f] [3].
[g] [17].

applied the same assumptions in our extrapolation from the rat to the human.

Model simulations of exhaled breath in humans (Fig. 6) are generally similar to observed data, supporting the validity of the IVIVE approach used to estimate the metabolism parameters in the model. However, this comparison allows assessment of only the systemically relevant pharmacokinetic drivers, e.g., partitioning and total metabolic clearance.

4.1. Future model enhancements

Several data gaps were identified during the development of the present PBPK model; filling of these data gaps would aid in refinement of a regionally-specific BD lung model. Metabolic rate constants used in this model were scaled from existing measurements of whole lung homogenate rather than in single cell types (club cells) or regional tissue samples. Additionally, while club cells are the primary metabolically active cells in pulmonary tissue, Type II cells, alveolar macrophages, and capillary endothelial cells may also be metabolically active, with enzymatic activity differences of 2- to 20-fold for various enzymes/species (reviewed briefly by [50]). Metabolic rate constants for downstream BD metabolites (e.g., BD-diol) also need to be further elucidated in order to support prediction of the urinary biomarkers identified in the literature. Time-course information on BD metabolite concentration profiles in rodent and human urine could then be used to refine the parameterization and to evaluate model predictions of BD and metabolite dosimetry for long-term exposures.

Conflict of Interest

The authors with the exception of Dr. Crowell are either employees of British American Tobacco or RJ Reynolds Tobacco Company, or are contractors to the aforementioned companies. All work was funded by British American Tobacco (Investments) Ltd and RJ Reynolds Tobacco Company. The Authors declare that no financial or personal conflicts of interest exist with regard to the submission of this manuscript.

Table A-4
Metabolic rate constants for the 1,3-butadiene PBsPK model.

Parameter	Symbol	Units	Rat	Mouse	Human
Max metabolic rate for CYP-mediated BD → EB in the liver	VMAXCYPL	nmol/min/mg protein	2.17[a]	2.59[b]	0.23[c]
Max metabolic rate for CYP-mediated BD → EB in the lung	VMAXCYPLU	nmol/min/mg protein	0.16[b]	2.31[b]	0.15[b]
Max metabolic rate for CYP-mediated BD → EB in the kidney	VMAXCYPK	nmol/min/mg protein	0.21[b]	2.31[b]	0.15[d]
Max conjugation rate for EB → EB-GSH in liver	VMAXGSHL	nmol/min/mg protein	241[b]	500[b]	45.1[b]
Max Conjugation Rate for EB → EB–GSH in lung	VMAXGSHLU	nmol/min/mg protein	44.2[b]	273[b]	8.3[b]
Max conjugation rate for EB → EB–GSH in kidney	VMAXGSHK	nmol/min/mg protein	44.2[b]	273[b]	8.3[b]
Max hydrolyzation rate for EB → BD-diol in liver	VMAXEHL	nmol/min/mg protein	17.0[a]	19.0[a]	3.1[c]
Max hydrolyzation rate for EB → BD-diol in lung	VMAXEHLU	nmol/min/mg protein	0.71[e]	0.58[e]	3.1[d]
Max hydrolyzation rate for EB → BD-diol in kidney	VMAXEHK	nmol/min/mg protein	0.25[e]	1.88[e]	3.1[d]
Max metabolic rate for CYP-mediated EB → DEB in the liver	VMAXEBCYPL	nmol/min/mg protein	0.41[f]	1.3[f]	0.915[c]
Max metabolic rate for CYP-mediated EB → DEB in Clara cells	VMAXEBCYPLU	nmol/min/mg protein	0.41[d]	1.3[d]	0.164[e]
Max metabolic rate for CYP-mediated EB → DEB in kidney	VMAXEBCYPK	nmol/min/mg protein	0.41[d]	1.3[d]	0.21[e]
Max metabolic rate for CYP-mediated BDIOL in the liver	MAXCYPBDIOLL	nmol/min/mg protein	1.12[e]	0.27[e]	3.1[c]
Max metabolic rate for CYP-mediated BDIOL in the lung	MAXCYPBDIOLLU	nmol/min/mg protein	0.53[e]	0.02[e]	3.1[d]
Max metabolic rate for CYP-mediated BDIOL in the kidney	MAXCYPBDIOK	nmol/min/mg protein	1.42[e]	0.02[e]	3.1[d]
Affinity constant for CYP-mediated BD → EB in lung	KMCYP	nmol/ml	3.75[b]	5.0[b]	0.7[j]
Affinity constant for CYP-mediated BD → EB in liver	KMCYPL	nmol/ml	7.75[b]	2.0[b]	0.7[b]
Affinity constant for CYP-mediated BD → EB in kidney	KMCYPK	nmol/ml	7.75	5.0[d]	0.7[j]
Affinity constant for CYP-mediated EB → DEB	KMEBCYP	nmol/ml	15.6[b]	15.6[b]	880[e]
Affinity constant for CYP-mediated EB → DEB in liver	KMEBCYPL	nmol/ml	15.6[d]	15.6[d]	880[k]
Affinity constant for CYP-mediated EB → DEB in kidney	KMEBCYPK	nmol/ml	15.6[d]	15.6[d]	880[k]
Affinity constant for EH-med. EB → BD-diol	KMEH	nmol/ml	140[a]	300[a]	540[c]
Affinity constant for EH-med. EB → BD-diol in liver	KMEHL	nmol/ml	140[d]	300[d]	540[k]
Affinity constant for EH-med. EB → BD-diol in kidney	KMEHK	nmol/ml	140[d]	300[d]	540[k]
Affinity constant for GSH conjugation, GST–GSH	KMGSH	nmol/ml	100[a]	100[a]	100[j]
Affinity constant for GSH conjugation, GST–EB in the liver	KMEBL	nmol/ml	13,800[b]	35,300[b]	10,400[b]
Affinity constant for GSH conjugation, GST–EB in the lung	KMEBLU	nmol/ml	17,400[b]	36,500[b]	10,400[d]
Affinity constant for GSH conjugation, GST–EB in the kidney	KMEBK	nmol/ml	13,800[d]	35,300[d]	10,400[d]
Basal degradation rate for GSH	KEGSH	1/min	0.0025[a]	0.0048[a]	0.012[c]
Initial GSH concentration in liver	CGSHL0	nmol/ml	6120.0[b]	8300.0[b]	6000.0[c]
Initial GSH concentration in richly perfused tissues	CGSHR0	nmol/ml	2000.0[e]	2000.0[j]	2000.0[j]
Initial GSH concentration in conducting airway tissue	CGSHCA0	nmol/ml	1580.0[g]	1580.0[j]	1580.0[j]
Initial GSH concentration in transitional airway tissue	CGSHTA0	nmol/ml	1580.0[g]	1580.0[j]	1580.0[j]
Initial GSH concentration in pulmonary tissue	CGSHP0	nmol/ml	1580.0[g]	1580.0[j]	1580.0[j]
Initial GSH concentration in kidney tissue	CGSHK0	nmol/ml	2240.0[g]	2240.0[j]	2240.0[j]
Release of EB from privileged access	KRELEB	1/min	1.4[m]	1.4[j]	1.4[j]
Microsomal protein content in liver	MMPPGL	mg/g	45.0[h]	45.0[j]	40.0[g]
Microsomal protein content in lung	MMPPGLU	mg/g	7.7[i]	7.7[d]	2.27[l]
Microsomal protein content in kidney	MMPPGK	mg/g	7.7[k]	7.7[d]	2.27[k]
Cytosolic protein content in liver	MCPPGL	mg/g	91.0[g]	91.0[j]	80.7[g]
Cytosolic protein content in lung	MCPPGLU	mg/g	38.0[h]	38.0[j]	38.0[j]
Cytosolic protein content in kidney	MCPPGK	mg/g	38.0[k]	38.0[j]	38.0[j]

[a] [27].
[b] [12].
[c] [59].
[d] Set to liver.
[e] [34].
[f] Seaton et al. [56].
[g] [53].
[h] [22].
[i] Yoon et al. [65].
[j] Set to rat value.
[k] Set to lung.
[l] [54].
[m] Estimated to minimize ratio of model to measured plasma EB AUC in rat.

Transparency Document

The Transparency document associated with this article can be found in the online version.

Acknowledgments

The authors would like to thank Dr. Susan Crowell and colleagues at Pacific Northwest National Laboratory (PNNL) for providing us with the code of their 1,3-butadiene model. The PBPK model described in this paper is an extension of their initial work. We would also like to thank Ms. Allison Franzen for her work on this project.

Appendix .

See Tables A-1 to A-4.

References

[1] R.J. Albertini, R.J. Sram, P.M. Vacek, J. Lynch, J.A. Nicklas, N.J. van Sittert, P.J. Boogaard, R.F. Henderson, J.A. Swenberg, A.D. Tates, J.B. Ward, M. Wright, Biomarkers in Czech workers exposed to 1,3-butadiene: a transitional epidemiologic study, Research Report 116, Health Effects Institute, Boston, MA, 2003.
[2] R. Beaudouin, S. Micallef, C. Brochot, A stochastic whole-body physiologically based pharmacokinetic model to assess the impact of inter-individual variability on tissue dosimetry over the human lifespan, Regul. Toxicol. Pharmacol. 57 (1) (2010) 103–116.
[3] F.Y. Bois, T.J. Smith, A. Gelman, H.-Y. Chang, A.E. Smith, Optimal design for a study of butadiene toxicokinetics in humans, Toxicol. Sci. 49 (1999) 213–224.
[4] H.M. Bolt, J.G. Filser, F. Stormer, Inhalation pharmacokinetics based on gas uptake studies, Arch. Toxicol. 55 (1984) 213–218.
[5] J.A. Bond, M.W. Himmelstein, M. Seaton, P. Boogaard, M.A. Medinsky, Metabolism of butadiene by mice, rats, and humans: a comparison of physiologically based toxicokinetic model predictions and experimental data, Toxicology 113 (1996) 48–54.
[6] J.A. Bond, M.A. Medinsky, Insights into the toxicodynamics of 1,3-butadiene, Chem. Biol. Interact. 135–136 (2001) 599–614.
[7] P.J. Boogaard, S.C-J. Sumner, J.A. Bond, Glutathione conjugation of 1,2:3,4-diepoxybutane in human liver and rat and mouse liver and lung *in vitro*, Toxicol. Appl. Pharmacol. 136 (1996) 307–316.
[8] C. Brochot, T.J. Smith, F.Y. Bois, Development of a physiologically based toxicokinetic model for butadiene and four major metabolites in humans: global sensitivity analysis for experimental design issues, Chem. Biol. Interact. 167 (2007) 168–183.
[9] R.P. Brown, M.D. Delp, S.L. Lindstedt, L.R. Rhomberg, R.P. Beliles, Physiological parameter values for physiologically based pharmacokinetic models, Toxicol. Ind. Health 13 (1997) 407–484.
[10] J. Butler, The bronchial circulation, in: C. Lenfant (Ed.), Lung Biology in Health and Disease, vol. 57, Marcel Dekker Inc., New York, 1992 (Chapter 5).
[11] M.S. Christian, Review of reproductive and developmental toxicity of 1,3-butadiene, Toxicology 113 (1–3) (1996) 137–143.
[12] G.A. Csanády, F.P. Guengerich, J.A. Bond, Comparison of the biotransformation of 1,3-butadiene and its metabolite, butadiene monoepoxide, by hepatic and pulmonary tissues from humans, rats and mice, Carcinogenesis 13 (7) (1992) 1143–1153.
[13] G.A. Csanády, P.E. Kreuzer, C. Baur, J.G. Filser, A physiological toxicokinetic model for 1,3-butadiene in rodents and man: blood concentrations of 1,3-butadiene, its metabolically formed epoxides, and of haemoglobin adducts – relevance of glutathione depletion, Toxicology 113 (1996) 300–305.
[14] E.L. Cussler, Diffusion: Mass Transfer in Fluid Systems, Cambridge University Press, Cambridge, UK, 1999.
[15] A.R. Dahl, R.F. Henderson, Comparative metabolism of low concentrations of butadiene and its monoepoxide in human and monkey hepatic microsomes, Inhal. Toxicol. 12 (2000) 439–451.
[16] R.J. Duescher, A.A. Elfarra, Human liver microsomes are efficient catalysts for 1,3-butadiene oxidation: evidence for major roles by cytochrome P450 2A6 and 2E1, Arch. Biochem. Biophys. 311 (1994) 342–349.
[17] J.G. Filser, G. Johanson, W. Kessler, P.F. Kreuzer, P. Stei, C. Baur, G.A. Csanady, A pharmacokinetic model to describe toxicokinetic interactions between 1,3-butadiene and styrene in rats: predictions for human exposure. IARC Scientific Publications No. 127 Butadiene and Styrene: Assessment of Health Hazards, 1993, p. 65–78.
[18] M.W. Himmelstein, M.J. Turner, B. Asgharian, J.A. Bond, Comparison of blood concentrations of 1,3-butadiene and butadiene epoxides in mice and rats exposed to 1,3-butadiene by inhalation, Carcinogenesis 15 (8) (1994) 1479–1486.
[19] M.W. Himmelstein, J.F. Acquavella, L. Recio, M.A. Medinsky, J.A. Bond, Toxicology and epidemiology of 1,3-butadiene, Crit. Rev. Toxicol. 27 (1) (1997) 100–108.
[20] M.W. Himmelstein, S.C. Carpenter, P.M. Hinderliter, Kinetic modeling of beta-chloroprene metabolism: I. *In vitro* rates in liver and lung tissue fractions from mice, rats, hamsters, and humans, Toxicol. Sci. 79 (1) (2004) 18–27.
[21] P.M. Hinderliter, K.D. Thrall, R.A. Corley, L.J. Bloemen, M.S. Bogdanffy, Validation of human physiologically based pharmacokinetic model for vinyl acetate against human nasal dosimetry data, Toxicol. Sci. 85 (2005) 460–467.
[22] J. Houston, A. Galetin, Methods for predicting *in vivo* pharmacokinetics using data from *in vitro* assays, Current Drug Metab. 9 (2008) 940–951.
[23] IARC, IARC monographs on the evaluation of carcinogenic risks to humans, vol. 97, 1,3-Butadiene, Ethylene Oxide and Vinyl Halides (Vinyl Fluoride, Vinyl Chloride and Vinyl Bromide), Lyon, France, 2008.
[24] ICRP, Human respiratory tract model for radiological protection. ICRP publication 66, Ann. ICRP. 24 (1–3) (1994) 1–11.
[25] R.S. Irwin, N. Augustyn, C.T. French, J. Rice, V. Tedeschi, S.J. Welch, Spread the word about the journal in 2013: from citation manipulation to invalidation of patient-reported outcomes measures to renaming the Clara cell to new journal features, Chest 143 (2013) 1–5, http://dx.doi.org/10.1378/chest.12-2762. PMID 23276834.
[26] T.E. Jackson, P.D. Lilly, L. Recio, P.M. Scholosser, M.A. Medinsky, Inhibition of cytochrome P450 2E1 decreases, but does not eliminate genotoxicity mediated by 1,3-butadiene, Toxicol. Sci. 55 (2000) 266–273.
[27] G. Johanson, J.G. Filser, A physiologically based pharmacokinetic model for butadiene and its metabolite butadiene monoxide in rat and mouse and its significance for risk extrapolation, Arch. Toxicol. 67 (1993) 151–163.
[28] G. Johanson, J.G. Filser, PBPK model for butadiene metabolism to epoxides: quantitative species differences in metabolism, Toxicology 113 (1996) 40–47.
[29] R.A. Kemper, A.A. Elfarra, S.R. Myers, Metabolism of 3-butene-1,2-diol in B6C3F1 mice evidence for involvement of alcohol dehydrogenase and cytochrome P450, Drug Metab. Dispos. 26 (9) (1998) 914–920.
[30] M.C. Kohn, The importance of anatomical realism for validation of physiological models of disposition of inhaled toxicants, Toxicol. Appl. Pharmacol. 147 (1997) 448–458.
[31] M.C. Kohn, R.L. Melnick, Species difference in the production and clearance of 1,3-butadiene metabolites: a mechanistic model indicates predominantly physiological, not biochemical, control, Carcinogenesis 14 (4) (1993) 619–628.
[32] M.C. Kohn, R.L. Melnick, Effects of the structure of a toxicokinetic model of butadiene inhalation exposure on computed production of carcinogenic intermediates, Toxicology 113 (1996) 31–39.
[33] M.C. Kohn, R.L. Melnick, The privileged access model of 1,3-butadiene disposition, Environ. Health Persp. 108 (5) (2000) 911–917.
[34] C.M. Kohn, R.L. Melnick, Physiological modeling of butadiene disposition in mice and rats, Chem. Biol. Interact. 135–136 (2001) 285–301.
[35] R. Krause, A.A. Elfarra, Oxidation of butadiene monoxide to meso- and (+/−)-diepoxybutane by cDNA-expressed human cytochrome P450s and by mouse, rat and human liver microsomes: evidence for preferential hydration of meso-diepoxybutane in rat and liver microsomes, Arch. Biochem. Biophys. 337 (1997) 176–184.
[36] R.J. Krause, J.E. Sharer, A.A. Elfarra, Epoxide hydrolase-dependent metabolism of butadiene monoxide to 3-butene-1,2-diol in mouse, rat, and human liver, Drug Metab. Dispos. 25 (8) (1997) 1013–1015.
[37] R. Kreiling, R.J. Laib, J.G. Filser, H.M. Bolt, Species differences in butadiene metabolism between mice and rats evaluated by inhalation pharmacokinetics, Arch. Toxicol. 58 (1986) 235–238.
[38] P.E. Kreuzer, W. Kessler, H.F. Welter, C. Baur, J.G. Filser, Enzyme specific kinetics of 1,2-epoxybutene-3 in microsomes and cytosol from livers of mouse, rat and man, Arch. Toxicol. 65 (1) (1991) 59–67.
[39] A.T. Mariassy, Chapter 6: epithelial cells of trachea and bronchi, in: R.A. Parent (Ed.), Comparative Biology of the Normal Lung, CRC Press, Boca Raton, FL, 1992.
[40] M.A. Medinsky, T.L. Leavens, G.A. Csanady, M.L. Gargas, J.A. Bond, *In vivo* metabolism of butadiene by mice and rats: a comparison of physiological model predictions and experimental data, Carcinogenesis 15 (7) (1994) 1329–1340.
[41] M.G. Menache, L.M. Hanna, E.A. Gross, S.-R. Lou, S.J. Zinreich, D.A. Leopold, A.M. Jarabek, F.J. Miller, Upper respiratory tract surface areas and volumes of laboratory animals and humans: considerations for dosimetry models, J. Environ. Sci. Health 50 (5) (1997) 475–506.
[42] R.R. Mercer, M.L. Russell, V.L. Roggli, J.D. Crapo, Cell number and distribution in human and rat airways, Am. J. Respir. Cell Mol. Biol. 10 (1994) 613–624.
[43] J. Myers, Emissions and monitoring trends of lower olefins across Texas from 2002–2012, in: Presented at the International Symposium: Evaluation of the Health Risks of Lower Olefins, Austin, TX, November 5–6, 2014.
[44] M.J. Oldham, R.F. Phalen, G.M. Schum, D.S. Daniels, Predicted nasal and tracheobronchial particle deposition efficiencies for the mouse, Ann. Occup. Hyg. 38 (1) (1994) 135–141.
[45] R.J. Pack, L.H. Al-Ugaily, G. Morris, J.G. Widdicombe, The distribution and structure of cells in the tracheal epithelium of the mouse, Cell Tissue Res. 208 (1) (1980) 65–84.
[46] R.J. Pack, L.H. Al-Ugaily, G. Morris, The cells of the tracheobronchial epithelium of the mouse: a quantitative light and electron microscope study, J. Anat. 132 (1981) 71–84.
[47] R.A. Parent (Ed.), Treatise on Pulmonary Toxicology, CRC Press, Boca Raton, FL, 1992.

[48] K.E. Pinkerton, P. Gehr, J.D. Crapo, Chapter 11: architecture and cellular composition of the air-blood barrier, in: R.A. Parent (Ed.), Comparative Biology of the Normal Lung, CRC Press, Boca Raton, FL, 1992.
[49] C.G. Plopper, L.H. Hill, A.T. Mariassy, Ultrastructure of the nonciliated bronchiolar epithelial (Clara) cell of mammalian lung. III. A study of man with comparison of 15 mammalian species, Exp. Lung Res. 1 (171) (1980) 180.
[50] C.G. Plopper, D.M. Hyde, A.R. Buckpitt, Clara cells, in: R.G. Crystal, J.B. West (Eds.), The Lung: Scientific Foundations, Raven Press, New York, 1991, pp. 527–534.
[51] C. Plopper, J. StGeorge, W. Cardoso, R. Wu, K. Pinkerton, A. Buckpitt, Relationship of cytochrome P-450 activity to Clara cell cytotoxicity. I. Histopathologic comparison of the respiratory tract of mice, rats and hamsters after parenteral administration of naphthalene., J. Pharmacol. Exp. Ther. 261 (1) (1992) 353–363.
[52] D.R. Plowchalk, M.E. Andersen, M.S. Bogdanffy, Physiologically based modeling of vinyl acetate uptake, metabolism and intracellular ph changes in the rat nasal cavity, Toxicol. Appl. Pharmacol. 142 (1997) 386–400.
[53] D.W. Potter, T.-B. Tran, Apparent rates of glutathione turnover in rat tissues, Toxicol. Appl. Pharmacol. 120 (1993) 186–192.
[54] R.A. Prough, Z. Sipal, S.W. Jakobsson, Metabolism of benzo(a)pyrene by human lung microsomal fractions, Life Sci. 21 (11) (1977) 1629–1635.
[55] R. Sarangapani, J.G. Teeguarden, G. Cruzan, H.J. Clewell, M.E. Andersen, Physiologically based pharmacokinetic modeling of styrene and styrene oxide respiratory-tract dosimetry in rodents and humans, Inhal. Toxicol. 14 (2002) 789–834.
[56] M.J. Seaton, C.G. Plopper, J.A. Bond, 1,3-Butadiene metabolism by lung airways isolated from mice and rats, Toxicology 113 (1996) 314–317.
[57] L.M. Sweeney, M.W. Himmelstein, P.M. Schlosser, M.A. Medinsky, Physiologically based pharmacokinetic modeling of blood and tissue epoxide measurements for butadiene, Toxicology 113 (1996) 318–321.
[58] L.M. Sweeney, P.M. Schlosser, M.A. Medinsky, J.A. Bond, Physiologically based pharmacokinetic modeling of 1,3-butadiene 1,2-epoxy-3-butene, and 1,2:3,4-diepoxybutane toxicokinetics in mice and rats, Carcinogenesis 18 (4) (1997) 611–625.
[59] L.M. Sweeney, M.W. Himmelstein, M.L. Gargas, Development of a preliminary physiologically based toxicokinetic (PBTK) model for 1,3-butadiene risk assessment, Chem. Biol. Interact. 135–136 (2001) 303–322.
[60] USEPA, Methods for derivation of inhalation reference concentrations and application of inhalation dosimetry, US Environmental Protection Agency, Office of Health and Environmental Assessment, EPA/600/8-90/066F, 1994.
[61] USEPA, Health assessment of 1,3-butadiene, National Center for Environmental Assessment – Washington Office. Office of Research and Development, U.S. Environmental Protection Agency, Washington, DC, EPA/600/P-98/001F, 2002.
[62] USEPA, Estimation programs interface suite™ for Microsoft® windows, v 4.11, United States Environmental Protection Agency, Washington, DC, USA, 2011.
[63] A. Winkelmann, T. Noack, The Clara cell: a "Third Reich eponym", Eur. Resp. J. 36 (2010) 722–727.
[64] H.C. Yeh, G.M. Schum, M.T. Duggan, Anatomic models of the tracheobronchial and pulmonary regions of the rat, Anat. Rec. 195 (1979) 483–492.
[65] M. Yoon, M.C. Madden, H.A. Barton, Developmental expression of aldehyde dehydrogenase in rat: a comparison of liver and lung development, Toxicol. Sci. 89 (2) (2006) 386–398.
[66] M. Yoon, J.L. Campbell, M.E. Andersen, H.J. Clewell, Quantitative *in vitro* to *in vivo* extrapolation of cell-based toxicity assay results, Crit. Rev. Toxicol. 42 (8) (2012) 633–652.